Kinetic Determination of Potassium Affinities by IRMPD: Elucidation of Precursor Ion Structures

Mathias Schäfer,*,† Miriam K. Drayss,† Dirk Blunk,† Jeremiah M. Purcell,‡,§ Christopher L. Hendrickson,§ Alan G. Marshall,§ Abhigya Mookherjee,|| and P. B. Armentrout||

Department of Chemistry, University of Cologne, Greinstrasse 4, 50939 Köln, Germany, Shell Global Solutions, Inc., Houston, Texas, National High Magnetic Field Laboratory, Florida State University, 1800 East Paul Dirac Drive, Tallahassee, Florida 32310-4005, and Department of Chemistry, University of Utah, Salt Lake City, Utah

Received: April 8, 2009; Revised Manuscript Received: May 18, 2009

Dissociation kinetics of the K^+ loss reaction of three potassiated tertiary amino acids (Scheme 1) were studied by infrared multiple photon dissociation (IRMPD) in a Fourier transform ion cyclotron resonance (FT ICR)-MS instrument. The aim of the study was to probe if a kinetic study by IRMPD can yield useful information on the ion structure of the precursor ion species. The measured activation energy values determined by IRMPD are related to the potassium affinity, ΔH_{K^+}, of *N*-methyl proline determined by threshold collision-induced dissociation experiments. By appropriate scaling with this reference value, the experimentally determined activation energy values for the K^+ loss are transformed into respective potassium affinities, $\Delta H_{K^+}^{IRMPD}$. These values match the calculated potassium affinity values for salt bridge (SB) structures, $\Delta H_{K^+}^{SB}$, substantially better than those for canonical structures with a single formal charge site (charge solvation (CS)), thereby allowing structure identification. This conclusion is consistent with other spectroscopic data, which yielded unambiguous evidence of these tertiary amino acids adopting SB structures in the gas phase. This study demonstrates that IRMPD can be applied to determine individual ion structures in the gas phase, given that adequate reference values are available for proper scaling.

Introduction

Dissociation kinetics studied by infrared multiple photon dissociation (IRMPD) experiments has proved to be an effective method for studying critical energies of fragmentation reactions.[1−9] For that purpose, the dissociation rate for the selected monomolecular fragmentation reaction is monitored as a function of the power density of the infrared laser used for precursor ion activation. It is important to note that the theoretical treatment of IRMPD relies on the broadly valid assumption that the excitation energy (absorbed infrared photons) is statistically distributed among the vibrational degrees of freedom of the photodissociating ion.[10] In addition, the fragmentation rate of the energized precursor ion has to be the rate determining step: that is, the dissociation reaction must be substantially slower than energy absorption and distribution. This latter criterion loses its validity, especially for smaller ions, and the high-energy tail of the Boltzmann distribution becomes depleted.[11] Dunbar introduced an approach for IRMPD of small ions (<50 atoms) based on a truncated Boltzmann distribution and a modified Tolman theorem to correct for the effect of reactive depletion of the precursor ion population.[11−14] With the simple Equation 1, the activation energy, E_a^{laser}, of the examined fragmentation reaction can be extracted from dissociation kinetics.[11]

$$E_a^{laser} = qh\nu \frac{d \ln k_{diss}}{d \ln P_{laser}} \quad (1)$$

In eq 1, q is the partition function for the vibrational mode that absorbs the incoming radiation, h is Planck's constant, ν is the laser frequency, k_{diss} is the first-order dissociation rate constant, and P_{laser} is the laser power density (W cm^{-2}). Because q varies slightly (between 1.01 and 1.1) with temperature, an average value of 1.05 was chosen for the maximum expected range of internal temperature (280−580 K) of the precursor ion.[1−4]

Experimental Section

Materials. *N*-methyl proline (R_1) and its four- and six-membered ring analogues *N*-methyl-azetidine-2-carboxylic acid (R_0) and *N*-methyl pipecolic acid (R_2) were synthesized according to a procedure described in detail elsewhere (Scheme 1).[15]

Infrared Radiative Multiphoton Dissociation (IRMPD) Experiments. All IRMPD experiments were conducted with a custom-built passively shielded 9.4 T electrospray ionization (ESI) Q FT-ICR instrument[16,17] configured for mass-selective external ion accumulation. The samples were infused at a flow rate of ∼300 nL/min through a 50 μm i.d. fused-silica microelectrospray emitter that had been mechanically ground to a uniform thin-walled tip.[18] General ESI conditions were: needle voltage, 2 kV; tube lens, 350 V; and heated metal capillary current, 4.0 A. The electrosprayed ions were transferred into the mass spectrometer through a Chait-style atmosphere-to-vacuum interface.[19] The ions traversed the heated metal capillary to the first stage of vacuum pumping into a skimmer region. The skimmer provides a conductance limit to the second

* Corresponding author. E-mail: mathias.schaefer@uni-koeln.de.
† University of Cologne.
‡ Shell Global Solutions, Inc.
§ Florida State University.
|| University of Utah.

10.1021/jp903232y CCC: $40.75
Published on Web 06/16/2009

SCHEME 1[a]

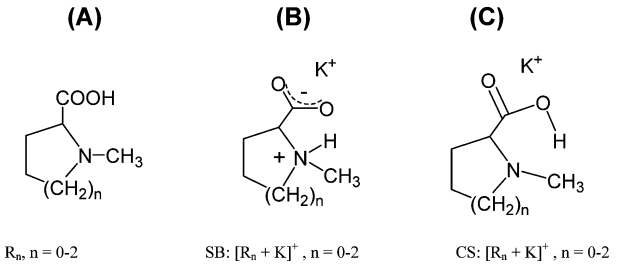

[a] (A) Neutral molecules, R_n, with $n = 0$ to 2 including *N*-methyl proline (R_1), (B) exemplary salt bridge (SB) structures, and (C) structures with a single formal charge site (canonical charge solvation (CS)) of potassiated molecular ions $[R_n + K]^+$ of R_n.

stage of differential pressure where the ions enter the first radio frequency (rf)-only octopole. In this first octopole, ions were accumulated for 1−30 s before transfer through a quadrupole (not operated in mass-resolving mode) into a second rf-only octopole, in which they were collisionally cooled (10−20 ms) with helium before transfer through an rf-only octopole to a 10 cm diameter, 30 cm long open cylindrical Penning ion trap.[20,21] The isotopic distribution of the potassiated precursor ions, $[R_n + K]^+$, was isolated by a combination of mass-selective external ion accumulation and stored waveform inverse Fourier transform (SWIFT) excitation.[22,23] The selected ions were then heated by infrared irradiation with a Synrad (model 48-2, Mukilteo, WA) 40 W continuous-wave CO_2 laser ($\lambda = 10^{-6}$ μm).[1−4] The factory-determined laser beam diameter is 3.5 mm. A 2.5× beam expander (to yield a beam diameter of ∼9 mm) was installed to ensure that the IR beam intercepted all of the stored ions in the ICR cell. Unfortunately, the minimum power density of the CO_2 laser was quite large (18.1 W cm^{-2}), which led to short irradiation periods ranging from only 0.5 to 3.2 s. Broadband frequency-sweep excitation (720 kHz to 7.2 MHz at 200 Hz/μs) accelerated the ions to a detectable cyclotron orbital radius. Ion cyclotron resonant frequencies were detected from induced differential current on two opposed detection electrodes of the ICR trap.[24,25] Ten time-domain acquisitions were summed for each sample, Hanning-apodized, and zero-filled once before fast Fourier transform and magnitude calculation. The experimental event sequence was controlled by a modular ICR data acquisition system (MIDAS).[26]

For IRMPD, the relative abundance of the precursor ion ($[R_n + K]^+/([R_n + K]^+ + [K]^+)$) was measured 10 times for each laser power density. Dissociation kinetics of the monomolecular fragmentation of the $[R_n + K]^+$ ions with $n = 0$ to 2 were determined for seven different laser power densities between 18.1 and 50.5 W cm^{-2}. First-order rate constants for the K^+-loss reaction of $[R_n + K]^+$ ions are determined by plotting the relative abundance of the respective precursor ion versus the irradiation period of the laser at individual power densities. Individual first-order rate constants for each laser power density are determined according to $k_{diss} = d \ln([R_n + K]^+/([R_n + K]^+ + [K]^+))/dt$. The IRMPD experiments were performed following protocols described in detail elsewhere.[3,4,27]

Threshold Collision-Induced Dissociation (TCID) Experiments. The potassium affinity (ΔH_{K^+}) of *N*-methyl proline (R_1) was determined by TCID in a guided ion beam tandem mass spectrometer.[28−32] The TCID experiments were performed following a protocol described in detail elsewhere.[28−30]

Computational Modeling. Identification and energy optimization of respective gas-phase ion structures of $[R_n + K]^+$ ions with $n = 0$ to 2 and of the neutral R_n molecules was achieved by computational modeling. CS and SB structures of the neutral molecules were combined with the K^+ ion and taken as input structures for a mixed low mode/Monte Carlo multiple minimum conformational search by use of MacroModel 8.1 (Schrodinger, Inc., Portland, OR). 5000 steps were performed, each followed by minimization with the Merck molecular force field (MMFF94s). Candidate structures with low MMFF energy were selected for higher level calculations. B3LYP computations proceeded with the 6-311++G(2d,2p) basis set on all atoms, as implemented in Gaussian 03.[33] Harmonic frequency calculations verified that all structures corresponded to local minima on the potential energy surface (PES) and provided zero-point energies (ZPEs). Basis set superposition errors (BSSEs) have been corrected by the counterpoise method.[34,35] To determine whether relative B3LYP energies agreed with more costly perturbation theory-based computations, optimization calculations at the MP2 level of theory (6-311++G(2d,2p)) were computed for all B3LYP structures. All relevant gas-phase ion structures of the $[R_n + K]^+$ ions are depicted in Figure 1. The structures of the respective neutral molecules, R_n, are depicted in Figure 2.[15,36] All illustrations of the energy-optimized gas-phase ion structures are generated with Chemcraft 1.5 and depicted as ball-and-stick models.

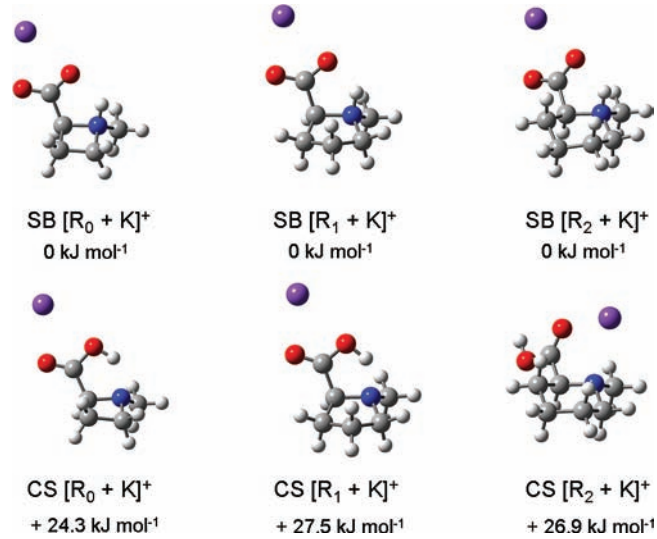

Figure 1. Most stable salt bridge (SB) and CS conformers of the potassiated molecular ions $[R_n + K]^+$ with $n = 0$, 1, 2 predicted by theory.

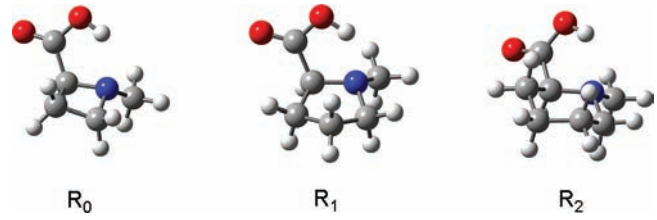

Figure 2. Most stable gas-phase structures of the neutral compounds R_n with $n = 0$, 1, 2 predicted by theory.

Results and Discussion

We now present an IRMPD study of potassiated *N*-methyl proline (R_1) and its four- and six-membered ring analogues, *N*-methyl-azetidine-2-carboxylic acid (R_0) and *N*-methyl-pipecolic acid (R_2) (specified number of methylene groups in the ring $n = 0$, 1, 2; see Scheme 1). A previous study with photoaction spectroscopy and ion mobility unambiguously

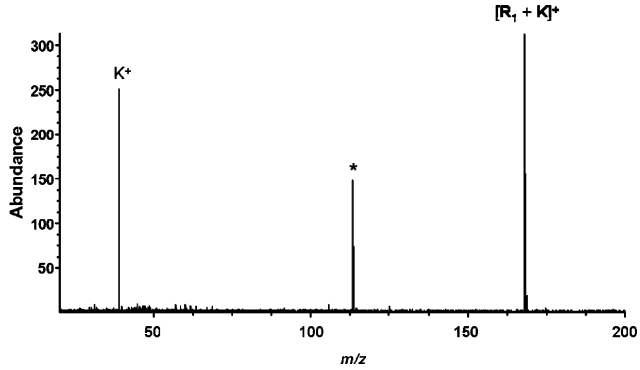

Figure 3. IRMPD spectrum of the potassiated *N*-methyl proline $[R_1 + K]^+$ at *m*/*z* 168. A CO_2 laser ($\lambda = 10.6\ \mu$m) was used for the IRMPD experiments. For the depicted spectrum, the precursor ion was irradiated for 1.3 s with a laser power density of 34.3 W cm^{-2}. * denotes electronic noise.

demonstrated that all compounds, R_n, adopt zwitterion structures in gas-phase $[R_n + K]^+$ ions.[15] Likewise, nonmethylated versions of all three ring systems have been shown to be zwitterionic.[28] All potassium adduct ions $[R_n + K]^+$ lose the respective neutral ligand molecule R_n upon IRMPD and deliver the potassium ion as the exclusive product ion. (See Figure 3.)[28]

The observation of this uniform fragmentation behavior makes it reasonable to assume that excitation of the dissociating precursor ions proceeds via energy exchange of comparable oscillators. Therefore, it is possible to establish a relative ordering of bond dissociation energies (BDEs), E_a^{laser}, for the disruption of the respective R_n-K^+ interaction by use of Equation 1.[2,3,5,6] Subsequently, the relative BDEs determined by IRMPD are quantitatively evaluated on the basis of the potassium affinity (ΔH_{K^+}) of *N*-methyl proline (R_1) determined by TCID in a guided ion beam tandem mass spectrometer.[28−32] Experimentally determined $\Delta H_{K^+}^{IRMPD}$ values are compared to calculated potassium affinity values to identify either SB or canonical charge solvation (CS) structures of R_n in $[R_n + K]^+$ ions (Schemes 1 and 2 and Table 1).

The outlined analytical strategy has obvious constraints, as Scheme 2 illustrates. First, the energy difference between alternative gas-phase ion structures for the $[R_n + K]^+$ ions (SB versus CS) has to be significantly larger than the experimental error of the IRMPD measurements. Table 1 shows that this is the case for all $[R_n + K]^+$ ions. (See Figures 1 and 2.) Second,

TABLE 1: Experimental and Theoretical Bond Dissociation Energies (Potassium Affinities, ΔH_{K^+}) for the Compounds $[R_n + K]^+$[a]

	$[R_0 + K]^+$	$[R_1 + K]^+$	$[R_2 + K]^+$
$\ln(k_{diss})/\ln(P_{laser})$[b]	2.46 ± 0.1	2.30 ± 0.15	2.37 ± 0.08
E_a^{laser} [c]	29.2 ± 1.0	27.4 ± 1.8	28.1 ± 1.0
$\Delta H_{K^+}^{IRMPD}$ [d]	158.6 ± 14.2	148.8 ± 15.7	152.6 ± 13.8
$\Delta H_{K^+}^{SB}$ [e]	147.4	154.9	151.9
$\Delta H_{K^+}^{CS}$ [e]	123.2	127.5	123.9
ΔH_{K^+}[f]		148.8 ± 7.6	

[a] All energy values are given in kilojoules per mole. [b] Slopes are derived from the linear fit in Figure 7; errors derived from linear fit. [c] E_a^{laser} values are calculated from eq 1. [d] $\Delta H_{K^+}^{IRMPD}$ values are calculated by multiplication of E_a^{laser} with scaling factor $M = 5.43 \pm 0.45$. [e] ΔH_{K^+} values calculated by DFT. [f] Potassium affinity value, ΔH_{K^+}, of *N*-methyl proline (R_1) measured by TCID.[28]

SCHEME 2: Schematic Description of the Potassium Loss Reaction of Potassiated *N*-Methyl Proline $[R_1 + K]^+$[a]

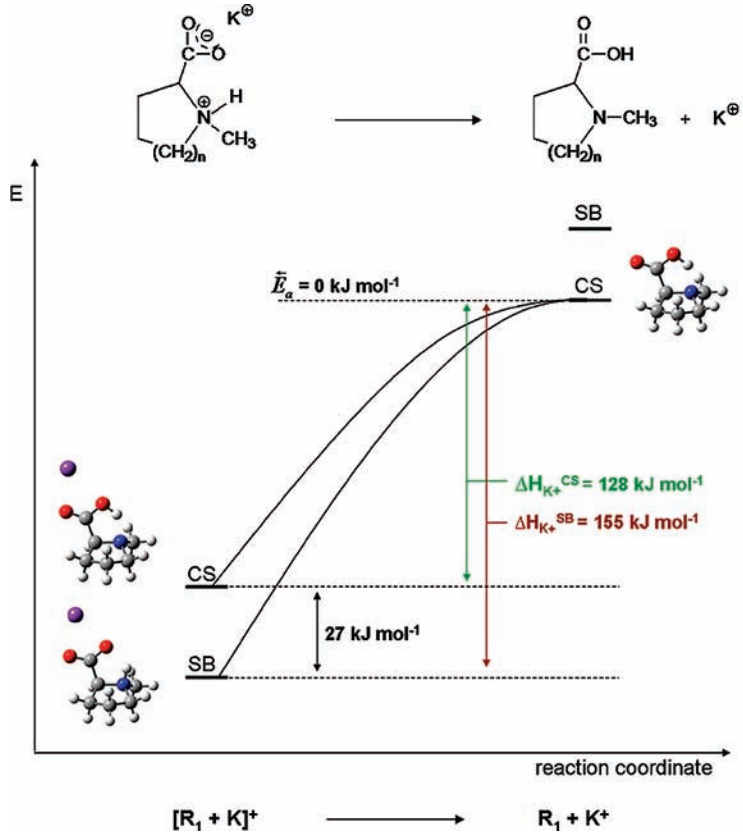

[a] Depicted salt bridge (SB) structure and the canonical structure with a single formal charge site (CS) of $[R_1 + K]^+$ and the structure of the neutral R_1 molecule are calculated by DFT (B3LYP/6-311++G(2d,2p)). The activation energy for the reverse reaction is assumed to be zero. Analogous reaction schemes are valid for compounds $[R_n + K]^+$ ions with $n = 0$, 2. (See Figures 1 and 2).

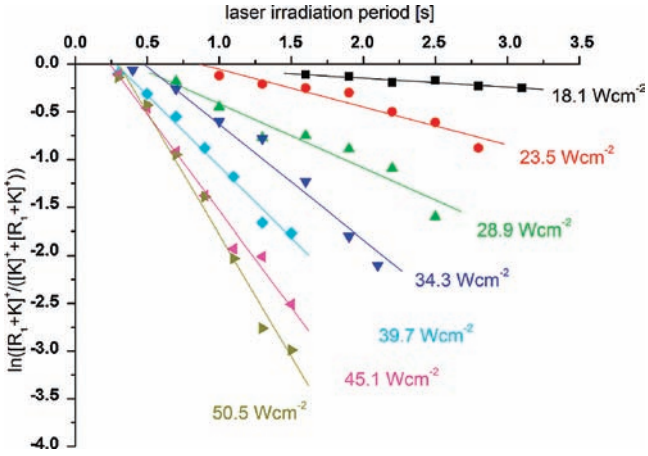

Figure 4. Plot of the natural logarithm of the relative abundance of the potassiated *N*-methyl praline $[R_1 + K]^+$ versus laser irradiation period for seven laser power densities.

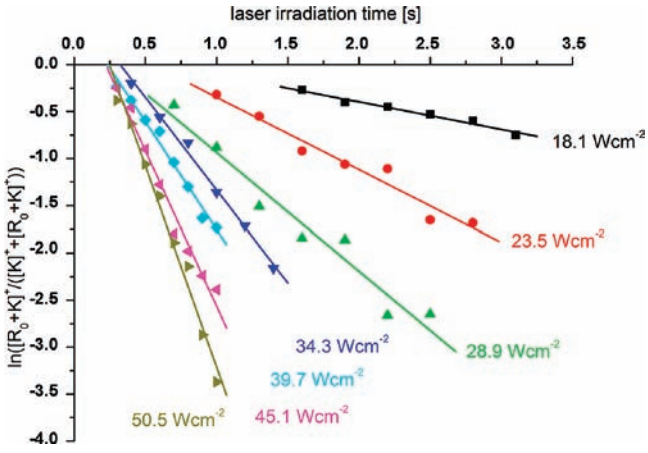

Figure 5. Plot of the natural logarithm of the relative abundance of the precursor ion $[R_0 + K]^+$ versus the laser irradiation period for seven laser power densities.

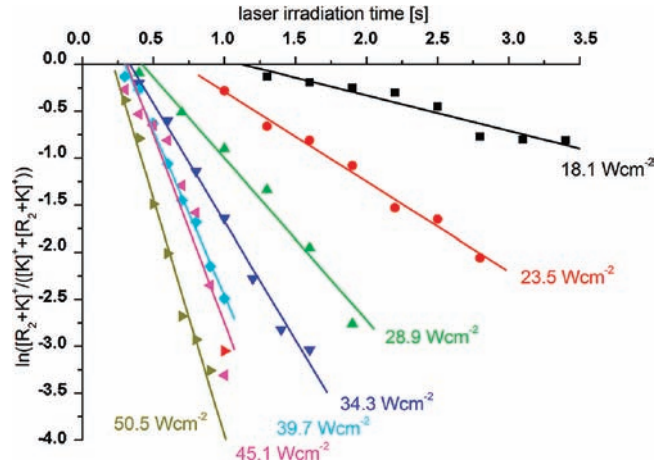

Figure 6. Plot of the natural logarithm of the relative abundance of the precursor ion $[R_2 + K]^+$ versus the laser irradiation period for seven laser power densities. The data point (▲) in red in the plot of P_{laser} 50.5 W cm^{-2} was not used for the linear fit because of excessive deviation.

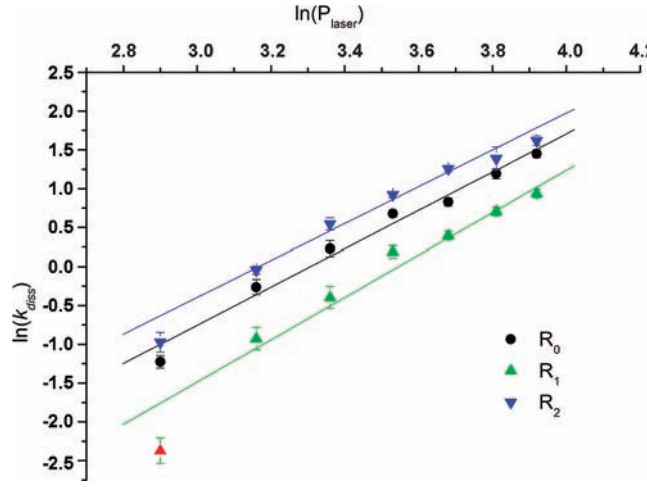

Figure 7. Natural logarithm of the first-order dissociation rate constant, k_{diss} [s^{-1}], for each respective laser power density versus the natural logarithm of the laser power density, P_{laser} [W cm^{-2}], for the precursor ions $[R_n + K]^+$ with $n = 0$ to 2. The data point (▲) in red in the plot of $[R_1 + K]^+$ was not used for the linear fit because of excessive deviation (>3 standard deviations). The error bars of the individual k_{diss} values are derived from the linear fit in Figures 4, 5, and 6.

the activation energy for the reverse reaction is assumed to be zero. Because K^+ is bound by weak electrostatic forces to the molecules R_n in the photodissociating complex ions $[R_n + K]^+$, the potassium loss reaction can be described by a simple dissociation mechanism without a substantial rearrangement of atoms in the R_n molecules.[29,30,37] Because loose (late) transition states (TSs) are typical for this kind of dissociation process, a reverse activation energy of zero is justified (Scheme 2).[29,30]

In Figure 7, the natural logarithm of the dissociation rate constant, k_{diss} (extracted from Figures 4, 5, and 6, respectively), for each respective laser power density is plotted versus the natural logarithm of the laser power density for each of the three $[R_n + K]^+$ ions. From eq 1, relative activation energy, E_a^{laser}, values for the potassium loss reaction of the three precursor ions $[R_n + K]^+$ are calculated (Table 1). The activation energies measured are very low. However, the individual E_a^{laser} values of the $[R_n + K]^+$ ions are, within the uncertainty of the method, quite similar, a result also found for potassium affinities determined for the unmethylated analogues by TCID.[28]

To determine an appropriate scaling factor for quantitative evaluation of the relative BDEs, an absolute potassium affinity value is needed. For that purpose, the absolute BDE of *N*-methyl proline (R_1) was measured ($\Delta H_{K^+} = 148.8 \pm 7.6$ kJ mol^{-1}) by TCID.[28] With that ΔH_{K^+} reference value, a scaling factor, *M*, was determined to be 5.43. By propagation of errors, the scaling factor, *M*, has an uncertainty of 0.45. The product of *M* with respective E_a^{laser} values of R_0 and R_2 gave the potassium affinity values, $\Delta H_{K^+}^{IRMPD}$, listed in Table 1. The IRMPD strategy relies on adequate reference values for proper scaling. Table 1 thus convincingly shows that TCID is the method of choice for high-precision determination of metal ion affinities.

By appropriate scaling, the experimentally determined BDEs, E_a^{laser}, are transformed into respective potassium affinities, $\Delta H_{K^+}^{IRMPD}$. These values for the R_n molecules match the calculated $\Delta H_{K^+}^{SB}$ values for SB structures substantially better than those for CS structures, thereby allowing structure identification (Table 1). This conclusion is consistent with other spectroscopic data, which yielded unambiguous evidence of compounds R_n adopting zwitterion structures (SB) in gas-phase $[R_n + K]^+$ ions.[15]

Although the precision of the present results does not provide meaningful results regarding the relative values for the three $\Delta H_{K^+}^{IRMPD}$ values determined here, it is interesting to note that theory finds that the $n = 1$ complex is bound more strongly than either $n = 0$ or 2. This trend is in agreement with the

experimental and theoretical results for the corresponding nonmethylated cyclic amino acids as well.[28] In that work, this was explained by the steric constraints associated with the smaller ring ($n = 0$) and by the observation that ring distortion was needed for the larger ring ($n = 2$) to form a strong hydrogen bond between the carboxylate and the protonated nitrogen center. In contrast, the five-membered ring ($n = 1$) forms this hydrogen bond with little change in the ring conformation. The present theoretical calculations provide parallel results.

Acknowledgment. This work was supported by NSF Division of Materials Research through DMR-0654118 and the State of Florida and the German Science Foundation (DFG). The generous provision of computing power at the Regional Computing Centre RRZK, Cologne, Germany, and in the frame of the D-GRID initiative is gratefully acknowledged. P.B.A. acknowledges the National Science Foundation, grant no. CHE-0748790.

References and Notes

(1) Freitas, M. A.; Hendrickson, C. L.; Marshall, A. G. *Rapid Commun. Mass Spectrom.* **1999**, *13*, 1639.

(2) Freitas, M. A.; Hendrickson, C. L.; Marshall, A. G. *J. Am. Chem. Soc.* **2000**, *122*, 7768.

(3) Schäfer, M.; Schmuck, C.; Geiger, L.; Chalmers, M. J.; Hendrickson, C. L.; Marshall, A. G. *Int. J. Mass Spectrom.* **2004**, *237*, 33.

(4) Schäfer, M.; Schmuck, C.; Heil, M.; Cooper, H. J.; Hendrickson, C. L.; Chalmers, M. J.; Marshall, A. G. *J. Am. Soc. Mass Spectrom.* **2003**, *14*, 1282.

(5) Flora, J. W.; Muddiman, D. C. *J. Am. Soc. Mass Spectrom.* **2004**, *15*, 121.

(6) Hannis, J. C.; Muddiman, D. C. *Int. J. Mass Spectrom.* **2002**, *219*, 139.

(7) Flora, J. W.; Muddiman, D. C. *J. Am. Chem. Soc.* **2002**, *124*, 6546.

(8) Leslie, A. D.; Daneshfar, R.; Volmer, D. A. *J. Am. Soc. Mass Spectrom.* **2007**, *18*, 632.

(9) Paech, K.; Jockusch, R. A.; Williams, E. R. *J. Phys. Chem. A* **2002**, *106*, 9761.

(10) Dunbar, R. C. *Int. J. Mass Spectrom.* **2000**, *200*, 571.

(11) Dunbar, R. C. *J. Chem. Phys.* **1991**, *95*, 2537.

(12) Dunbar, R. C.; Zaniewski, R. *J. Chem. Phys.* **1992**, *96*, 5069.

(13) Uechi, G. T.; Dunbar, R. C. *J. Chem. Phys.* **1992**, *96*, 8897.

(14) Uechi, G. T.; Dunbar, R. C. *J. Chem. Phys.* **1993**, *98*, 7888.

(15) Drayss, M. K.; Blunk, D.; Oomens, J.; Gao B.; Wyttenbach, T.; Bowers, M. T.; Schäfer, M. *J. Phys. Chem. A* **2009**, submitted.

(16) Senko, M. W.; Hendrickson, C. L.; Pasa-Tolic, L.; Marto, J. A.; White, F. M.; Guan, S.; Marshall, A. G. *Rapid Commun. Mass Spectrom.* **1996**, *10*, 1824.

(17) Hakansson, K.; Chalmers, M. J.; Quinn, J. P.; McFarland, M. A.; Hendrickson, C. L.; Marshall, A. G. *Anal. Chem.* **2003**, *75*, 3256.

(18) Quinn, J. P.; Emmett, M. R.; Marshall, A. G. In *Proceedings of the 46th ASMS Conference on Mass Spectrometry and Allied Topics*, Orlando, FL, May 31−June 4, 1998; p 1388.

(19) Chowdhury, S. K.; Katta, V.; Chait, B. T. *Rapid Commun. Mass Spectrom.* **1990**, *4*, 81.

(20) Senko, M. W.; Hendrickson, C. L.; Emmett, M. R.; Shi, S. D. H.; Marshall, A. G. *J. Am. Soc. Mass Spectrom.* **1997**, *8*, 970.

(21) Beu, S. C.; Laude, D. A., Jr. *Int. J. Mass Spectrom. Ion Processes* **1992**, *112*, 215.

(22) Marshall, A. G.; Wang, T.-C. L.; Ricca, T. L. *J. Am. Chem. Soc.* **1985**, *107*, 7893.

(23) Guan, S.; Marshall, A. G. *Int. J. Mass Spectrom. Ion Processes* **1996**, *157/158*, 5.

(24) Comisarow, M. B.; Marshall, A. G. *Chem. Phys. Lett.* **1974**, *26*, 489.

(25) Marshall, A. G.; Roe, D. C. *J. Chem. Phys.* **1980**, *73*, 1581–1590.

(26) Senko, M. W.; Canterbury, J. D.; Guan, S.; Marshall, A. G. *Rapid Commun. Mass Spectrom.* **1996**, *10*, 1839.

(27) Håkansson, K.; Chalmers, M. J.; Quinn, J. P.; McFarland, M. A.; Hendrickson, C. L.; Marshall, A. G. *Anal. Chem.* **2003**, *75*, 3256.

(28) Moision, R. M.; Armentrout, P. B. *J. Phys. Chem. A* **2006**, *110*, 3933.

(29) Heaton, A. L.; Armentrout, P. B. *J. Phys. Chem. B* **2008**, *112*, 12056.

(30) Armentrout, P. B.; Ervin, K. M.; Rodgers, M. T. *J. Phys. Chem. A* **2008**, *112*, 10071.

(31) Ervin, K. M.; Armentrout, P. B. *J. Chem. Phys.* **1985**, *83*, 166.

(32) Muntean, F.; Armentrout, P. B. *J. Chem. Phys.* **2001**, *115*, 1213.

(33) Frisch, M. J.; Trucks, G. W.; Schlegel, H. B.; Scuseria, G. E.; Robb, M. A.; Cheeseman, J. R.; Montgomery, J. A., Jr.; Vreven, T.; Kudin, K. N.; Burant, J. C.; Millam, J. M.; Iyengar, S. S.; Tomasi, J.; Barone, V.; Mennucci, B.; Cossi, M.; Scalmani, G.; Rega, N.; Petersson, G. A.; Nakatsuji, H.; Hada, M.; Ehara, M.; Toyota, K.; Fukuda, R.; Hasegawa, J.; Ishida, M.; Nakajima, T.; Honda, Y.; Kitao, O.; Nakai, H.; Klene, M.; Li, X.; Knox, J. E.; Hratchian, H. P.; Cross, J. B.; Bakken, V.; Adamo, C.; Jaramillo, J.; Gomperts, R.; Stratmann, R. E.; Yazyev, O.; Austin, A. J.; Cammi, R.; Pomelli, C.; Ochterski, J. W.; Ayala, P. Y.; Morokuma, K.; Voth, G. A.; Salvador, P.; Dannenberg, J. J.; Zakrzewski, V. G.; Dapprich, S.; Daniels, A. D.; Strain, M. C.; Farkas, O.; Malick, D. K.; Rabuck, A. D.; Raghavachari, K.; Foresman, J. B.; Ortiz, J. V.; Cui, Q.; Baboul, A. G.; Clifford, S.; Cioslowski, J.; Stefanov, B. B.; Liu, G.; Liashenko, A.; Piskorz, P.; Komaromi, I.; Martin, R. L.; Fox, D. J.; Keith, T.; Al-Laham, M. A.; Peng, C. Y.; Nanayakkara, A.; Challacombe, M.; Gill, P. M. W.; Johnson, B.; Chen, W.; Wong, M. W.; Gonzalez, C.; Pople, J. A. *Gaussian 03*, revision D.01; Gaussian, Inc.: Pittsburgh, PA, 2005.

(34) Simon, S.; Duran, M.; Dannenberg, J. J. *J. Chem. Phys.* **1996**, *105*, 11024.

(35) Boys, S. F.; Bernardi, F. *Mol. Phys.* **1970**, *19*, 553.

(36) Drayss, M. K.; Blunk, D.; Oomens, J.; Schäfer, M. *J. Phys. Chem. A* **2008**, *112*, 11972.

(37) Armentrout, P. B.; Simons, J. *J. Am. Chem. Soc.* **1992**, *114*, 8627.

JP903232Y